Vortex ratchet induced by controlled edge roughness

D Cerbu[1,6], **V N Gladilin**[1,2], **J Cuppens**[1,5], **J Fritzsche**[3],
J Tempere[2], **J T Devreese**[2], **V V Moshchalkov**[1], **A V Silhanek**[4]
and J Van de Vondel[1]

[1] INPAC—Institute for Nanoscale Physics and Chemistry, KU Leuven,
Celestijnenlaan 200D, B-3001 Leuven, Belgium
[2] TQC—Theory of Quantum and Complex Systems, Universiteit Antwerpen,
Universiteitsplein 1, B-2610 Antwerpen, Belgium
[3] Department of Applied Physics, Chalmers University of Technology,
SE-412 96 Göteborg, Sweden
[4] Département de Physique, Université de Liège, Allée du 6 août 17, Bat. B5a,
B-4000 Sart Tilman, Belgium
E-mail: dorin.cerbu@fys.kuleuven.be

Abstract. We demonstrate theoretically and experimentally the generation
of rectified mean vortex displacement resulting from a controlled difference
between the surface barriers at the opposite borders of a superconducting strip.
Our investigation focuses on Al superconducting strips where, in one of the two
sample borders, a saw tooth-like array of micro-indentations has been imprinted.
The origin of the vortex ratchet effect is based on the fact that (i) the onset
of vortex motion is mainly governed by the entrance/nucleation of vortices
and (ii) the current lines bunching produced by the indentations facilitates the
entrance/nucleation of vortices. Only for one current direction the indentations
are positioned at the side of vortex entry and the onset of the resistive regime is
lowered compared to the opposite current direction. This investigation points to
the relevance of ubiquitous border effects typically neglected when interpreting
vortex ratchet measurements on samples with arrays of local asymmetric pinning
sites.

[5] Present address: Department of Condensed Matter Physics, Weizmann Institute of Science, Rehovot 76100, Israel.
[6] Author to whom any correspondence should be addressed.

Contents

1. Introduction

Mobile physical entities such as particles, bacteria or water droplets, subjected to a zero mean periodic excitation, can acquire a finite mean momentum if the energy potential landscape is asymmetric [1–4]. A particularly attractive system for testing these non-equilibrium phenomena can be made on the basis of type-II superconductors where the quantum bundles of magnetic flux can be regarded as repulsively interacting particles in an energy potential landscape fully determined by the inhomogeneities of the superconducting condensate [5, 6]. The possibility of changing the number of particles by simply changing the magnetic field intensity or of tuning the size of the particles by properly adjusting the temperature makes this superconducting system an ideal toy model. In general, for isolated particles, rectification is obtained when the typical distance traveled by the particles during the period of the excitation is larger than the length scale at which the symmetry of the potential is broken. However, the response of the system becomes more complex at high densities, when the separation between the particles is smaller than the length scale of the potential and their mutual interaction becomes important. For instance, multiple reversals of the easy-axis rectification direction can be observed as the number of particles is increased or when the characteristic length scale of the potential asymmetry changes [7–9].

The vast majority of the theoretical approaches for describing the physical mechanisms of these ratchet systems assume an infinite medium with no borders or with periodic boundary conditions. Neglecting sample borders in superconducting systems seems to be unjustified from an experimental point of view [10, 11] unless special care is taken to move the particles in circles such as in the Corbino disc configuration [12]. Indeed, it has been recognized in the past that unwanted differences between the two sample borders can lead to spurious rectification signals [13–17]. However, it still remains unclear whether there is also an influence from the asymmetric entering–exit process.

More than 50 years ago the work of Bean and Livingstone (BL) addressed the influence of the sample edge on the magnetic properties of a type-II superconductor [18]. In their seminal paper, they describe the presence of a surface barrier at a vacuum/superconducting interface arising from the competition between the repulsion of a vortex from the surface due to Meissner currents, and the attractive image force arising from the boundary condition of zero current normal to the sample edge.

This surface barrier, inherently present in finite superconducting samples, is not symmetric, i.e. the energy needed to introduce a vortex into the sample is different from that needed to remove the vortex from the sample. This difference between vortex nucleation and vortex exit leads to metastabilities that manifest themselves as hysteretic magnetization curves [19, 20]. Although in electrical transport experiments the BL barrier can be an important factor that determines the critical current (particularly in the weak pinning regime), the fact that vortex trajectories involve entering, traveling across the sample and exiting the sample implies that the most resistive mechanism (i.e. vortex entering) dominates. This asymmetry of the BL barrier could not yet be detected with ac transport measurements since, once again, both the entering and exiting processes take place at the same time for the vortex lattice independent of the current direction.

We will show that even though the asymmetry of the BL barrier does not constitute a sufficient condition to induce vortex rectification by electrical transport measurements, it is a necessary ingredient to achieve rectification. It is possible to create a vortex rectifier by lowering the barrier for vortex entry only on one side of the superconducting bridge while leaving the other side unchanged. Depending on the sign of the applied current, vortex entry can occur either at one or the other side of the bridge. As a result, only for one particular current direction the barrier for vortex entry is drastically reduced, which is manifested in a clear difference between the measured dissipation for both current directions.

In this paper, we study the impact of a micro fabricated roughness at the border of a superconducting thin film on the rectification of vortices. We investigate the difference in dc voltage (V_{dc}) response under an ac current drive, between a superconducting Al bridge with two equally straight edges and a bridge with an array of indentations only on one side of the bridge. The size of these saw tooth indentations has been chosen to be comparable with the size of the superconducting vortices. The experimental findings are in agreement with time-dependent Ginzburg–Landau (TDGL) simulations.

2. Sample details

We investigate superconducting Al thin films in strip geometry of $50 \, \mu\text{m}$ width, $200 \, \mu\text{m}$ length and $50 \, \text{nm}$ thickness. The fabrication was done by patterning a resist mask, on top of a SiO_2 substrate, with the help of electron beam lithography and then by deposition of an Al thin film by molecular beam epitaxy on top of the patterned resist mask and subsequent lift-off. Only at one side of the bridge a series of equally spaced triangular-shaped indentations were made. The dimensions of the fabricated samples are presented in figure 1. In order to check reproducibility and robustness of this type of vortex rectifier, we fabricated several samples with varying density of indentations. We focus here on the two extreme cases: the reference bridge with no indentations and the bridge with one indented side with maximum density of indents allowed by their size, having zero pitch between the indents.

According to the Drude model [21] the product ρl_{el} is a constant that depends on the material, where ρ and l_{el} are resistivity and electron mean free path, respectively. In [22] it has been shown that for thin aluminum films we have $\rho_{4K} l_{el} = 4 \times 10^{-16} \, \Omega \, \text{m}^2$. In our case the measured resistivity at $4 \, \text{K}$ is $\rho_{4K} = 1.425 \times 10^{-8} \, \Omega \, \text{m}$, which gives $l_{el} = 28 \, \text{nm}$. The dirty limit expressions [23] $\xi(T) = 0.855\sqrt{\xi(0)l_{el}/(1 - T/T_{c0})}$ and $\lambda(T) = 0.64\lambda_L(0)\sqrt{\xi(0)/l_{el}(1 - T/T_{c0})}$, where $\lambda_L(0)$ is the London penetration depth, result in a coherence length $\xi(0) = 181 \, \text{nm}$ and a penetration depth $\lambda(0) = 77 \, \text{nm}$ for the samples under
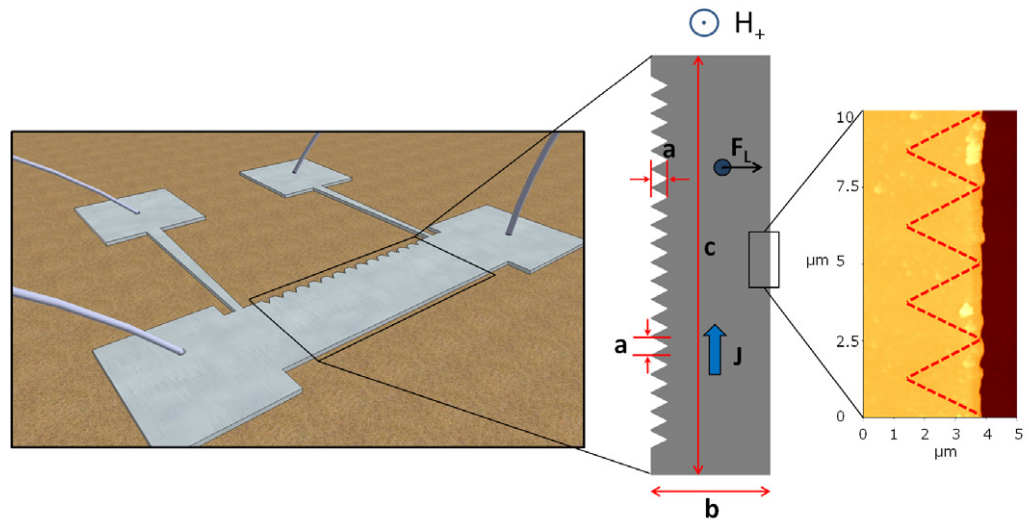
Figure 1. Superconducting aluminum thin film in bridge geometry. The side contacts are used for voltage probing and the current is injected through the contact pads at each end of the bridge. The geometrical parameters are $a = 2.5\,\mu$m, $b = 50\,\mu$m, $c = 200\,\mu$m and Al film thickness $t = 50$ nm. H, J and F_L are the applied magnetic field, the driving current density and the Lorentz force acting upon Abrikosov vortices, respectively. The directions of the magnetic field and driving current, as illustrated here, give the definitions for the positive applied values. At the right side of the figure, we have an atomic force microscopy image of the flat side of the Al bridge. The nominally flat border has imperfections such as protrusions sticking out by $0.25\,\mu$m. The red dashed lines illustrate for comparison the shape and size of the indents at the opposite side of the bridge.

investigation. The effective penetration depth $\Lambda(0) = \lambda^2(0)/t$ for the $t = 50$ nm thin film is $\Lambda(0) = 119$ nm. The critical temperature, determining the onset of superconductivity, is $T_{c0} = 1.285$ K.

3. Experimental results

The electrical measurements were carried out using a four-probe Kelvin configuration, with ac currents fed by a Keithley 6221 source whereas a Keithley 1228a digital nanovoltmeter was used for voltage probing. The $E_{dc}(j_{ac})$ characteristics for the studied samples are shown in figure 2. Here the applied magnetic field is 0.55 mT and the frequency of the ac current is $f = 33.711$ kHz. Taking into consideration that typically the vortex velocities are at least hundreds of meters per second [24], for micrometer-wide bridges the low applied driving frequency ensures that during half of the ac cycle the vortices travel across the entire bridge. The measurement was taken at temperature $T = 1.12$ K ($0.87\,T/T_{c0}$). The inset of figure 2 shows a zoom-in at lower current densities where the generated electrical field E_{dc} corresponds to a vortex ratchet and the easy direction of vortex ratchet motion is from left to right (see figure 1) in the indented bridge. The reference sample shows no vortex ratchet effect. In figure 2, we can clearly distinguish an E_{dc} peak at a current density roughly 30 kA cm^{-2} for the indented sample
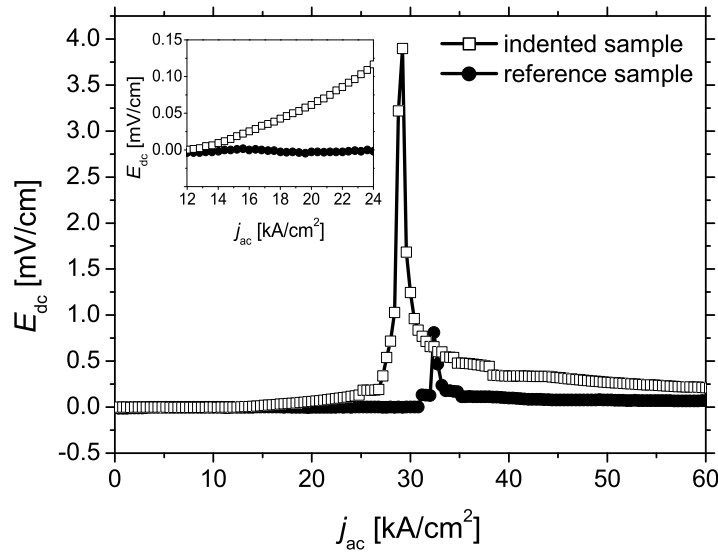
Figure 2. Comparison of the electric field–current $E_{dc}(j_{ac})$ characteristics for the reference and the indented samples. The inset shows a zoom of $E_{dc}(j_{ac})$ for low current density values at the onset of the resistive regime. Measurements were done in a magnetic field perpendicular to the film surface $H = 0.55\,\mathrm{mT}$ and for a driving frequency $f = 33.711\,\mathrm{kHz}$. The cryostat temperature during measurements was kept at $T = 1.12\,\mathrm{K}$.
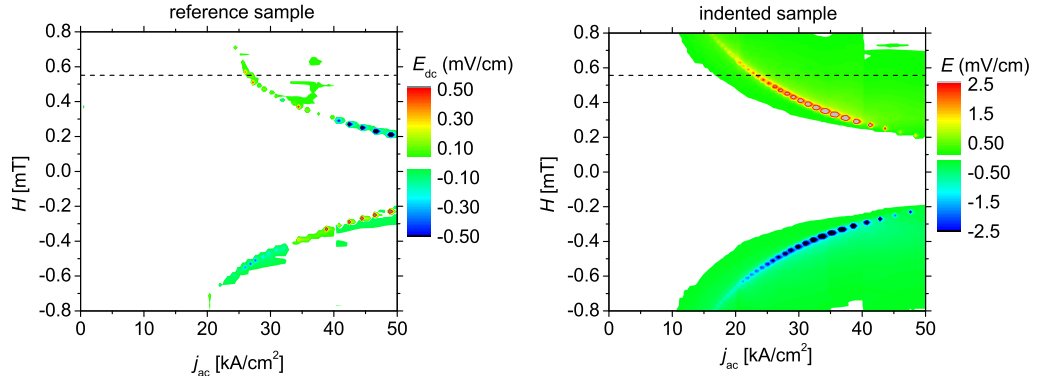
Figure 3. Contour plot, for the reference and indented samples, of the net dc electric field $E_{dc}(j_{ac}, H)$ as a function of the magnetic field and amplitude of the sinusoidal ac current density at a frequency 33 kHz and $T/T_{c0} = 0.87$. The dashed lines at $H = 0.55\,\mathrm{mT}$ indicate the conditions under which the data of figure 2 were obtained.

(open squares) and a much smaller peak at roughly $32\,\mathrm{kA\,cm^{-2}}$ for the reference sample (filled circles). The steep increase of E_{dc} has been attributed to the onset of phase slip lines (PSLs) once the vortex velocity reaches a critical value [25].

In figure 3 we have for both samples the obtained electric field versus current density $E_{dc}(j_{ac})$ measurements taken at $T = 1.12\,\mathrm{K}$ for different magnetic fields ranging from -0.8 to $0.8\,\mathrm{mT}$. These contour plots clearly demonstrate that the presence of indents induces the

rectification of vortex motion over a wide range of magnetic fields. In contrast to that, the reference sample exhibits a very weak rectification signal probably originating from unavoidable imperfections of the nominally flat sample borders, in agreement with previous reports [13, 14, 26] or from the fact that placing both voltage contacts at one side of the bridge leads also to breaking the inversion symmetry [27, 28].

The antisymmetric dependence on the magnetic field is explained by the inversion of the Lorentz force (and therefore also the vortex motion direction) when changing the polarity of the magnetic field-induced vortices. The rectification sign for all indented samples is identical, which indicates that the easy direction of vortex motion in these samples is the same. This shows that the indentations break the symmetry of vortex motion in a robust and systematic way.

4. Theoretical model

We describe vortex dynamics using the generalized TDGL equation for dirty superconductors [29]:

$$\frac{1}{\sqrt{1+\gamma^2|\psi|^2}}\left(\frac{\partial}{\partial t}+i\varphi+\frac{1}{2}\gamma^2\frac{\partial|\psi|^2}{\partial t}\right)\psi$$

$$=(\nabla-i\mathbf{A})^2\psi+2\left(1-\frac{T}{T_c}\right)\psi(1-|\psi|^2). \tag{1}$$

Here ψ is the order parameter, and φ and $\mathbf{A}$ are the scalar and vector potentials, respectively. The relevant quantities are made dimensionless by expressing lengths in units of $\sqrt{2}\xi(0)$, time in units of $\pi\hbar/(4k_BT_c)\approx11.6\tau_{GL}(0)$, magnetic field in units of $\Phi_0/(4\pi\xi^2(0))=H_{c2}(0)/2$, current density in units of $\Phi_0/[2\sqrt{2}\pi\mu_0\lambda^2(0)\xi(0)]=3\sqrt{3}/(2\sqrt{2})j_c(0)$ and scalar potential in units of $2k_BT_c/(\pi e)$. Here, $\Phi_0=\pi\hbar/e$ is the magnetic flux quantum, μ_0 is the vacuum permeability, τ_{GL} is the Ginzburg–Landau time, H_{c2} is the second critical field and j_c is the critical (depairing) current density of a thin wire or film [23].

The parameter $\gamma=8\tau_Ek_BT_c\sqrt{u(1-T/T_c)}/(\pi\hbar)$ is proportional to τ_E, the inelastic collision time for electron–phonon scattering. u is a numerical factor, which approximately equals 5.79 [29]. At $\gamma\gg1$ the healing time of the superconducting condensate is $\sim\gamma|\psi|\tau_{GL}$ (see e.g. [30]). Equation (1) is strictly valid for [29] $\gamma^2<u/(1-T/T_c)$, i.e. for $\gamma\lesssim10$ at $(1-T/T_c)\lesssim0.1$. At the same time, the γ value experimentally obtained for Al is as large as ~1000 for those temperatures [31]. Nevertheless, it appears that the approach, based on the use of equation (1) with $\gamma\sim10$, is able to capture the main physical mechanisms, related to the vortex dynamics in thin Al samples [32] as well as to the ratchet effect in Al bridges with arrays of asymmetric pinning sites [25]. In the present calculations, we take $\gamma=10$.

The distribution of the scalar potential φ that enters in equation (1) is determined from the condition
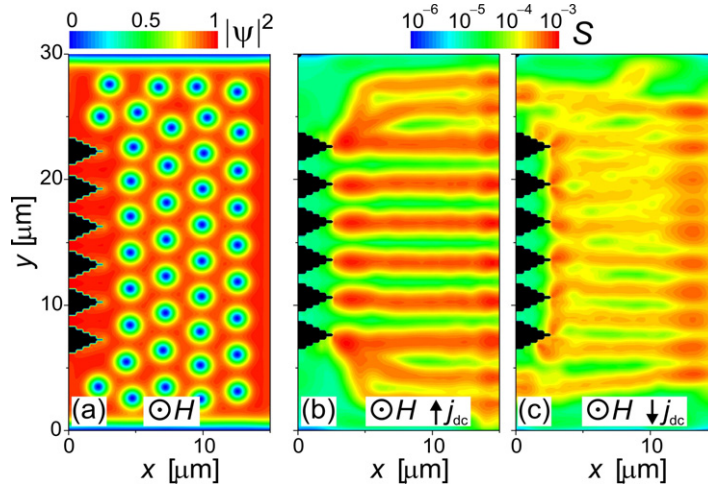
$$\nabla\cdot\mathbf{j}=0 \tag{2}$$

which reflects the continuity of currents in the superconductor. The total current density $\mathbf{j}$ is given by the sum of the normal and superconducting components:

$$\mathbf{j}=\mathbf{j}_n+\mathbf{j}_s, \tag{3}$$

$$\mathbf{j}_n=-\frac{\sigma}{2}\left(\nabla\varphi+\frac{\partial\mathbf{A}}{\partial t}\right), \tag{4}$$

Figure 4. (a) Calculated distribution of the square modulus of the order parameter in the absence of an applied current. Panels (b) and (c) show the distributions of the streaming parameter S for $t_2 - t_1 = 40\,000$ at positive ($j_{dc} = 43\,\text{kA cm}^{-2}$) and negative ($j_{dc} = -43\,\text{kA cm}^{-2}$) applied dc current, respectively.

$$\mathbf{j}_s = \left(1 - \frac{T}{T_c}\right)\left[\text{Im}\,(\psi^*\nabla\psi) - \mathbf{A}|\psi|^2\right], \tag{5}$$

where σ is the normal-state conductivity, which is taken as $\sigma = 1/12$ in our units [33]. The vector potential $\mathbf{A}$, for which we choose the gauge $\nabla \cdot \mathbf{A} = 0$, can be represented as

$$\mathbf{A} = \mathbf{A}_e + \mathbf{A}_s. \tag{6}$$

Here $\mathbf{A}_e$ denotes the vector potential corresponding to the externally applied magnetic field $\mathbf{H}$, while $\mathbf{A}_s$ describes the vector potential induced by the currents $\mathbf{j}$ that flow in the superconductor:

$$\mathbf{A}_s(\mathbf{r}) = \frac{1}{2\pi\kappa^2}\int \text{d}^3 r' \frac{\mathbf{j}(\mathbf{r}')}{|\mathbf{r} - \mathbf{r}'|}, \tag{7}$$

where $\kappa = \lambda/\xi$ is the Ginzburg–Landau parameter. Integration in equation (7) is performed over the volume of the superconductor.

In our model, we consider a thin superconducting strip (see figure 4(a)) with thickness 50 nm, lateral sizes $L_x \times L_y = 15\,\mu\text{m} \times 30\,\mu\text{m}$ (somewhat smaller than those for the experimental samples) and indentations similar to those in the experimental samples. An external homogeneous constant magnetic field H is perpendicular to the strip, while the external transport current is applied in the y-direction. The TDGL simulations are performed for $\xi(0) = 181\,\text{nm}$, $\lambda(0) = 77\,\text{nm}$, $T = 1.12\,\text{K}$, $T_c = 1.285\,\text{K}$ and $H = 0.55\,\text{mT}$. Since the thickness of the superconductor is significantly smaller than the coherence length $\xi(T)$, variations of the order-parameter magnitude across the layer as well as currents in this direction are negligible. For such a thin superconductor film, equations (1) and (2) can be rewritten in the xy-plane only, by replacing ∇ with $\nabla_{2D} \equiv \mathbf{e}_x \partial/\partial x + \mathbf{e}_y \partial/\partial y$ and $\mathbf{A}$ with $\langle\mathbf{A}_{2D}\rangle$, where $\mathbf{e}_x$ and $\mathbf{e}_y$ are unit vectors in the x- and y-directions, respectively, while $\langle\mathbf{A}_{2D}\rangle$ denotes the in-plane vector potential

averaged along the thickness of the superconductor. The superconductor–insulator boundary conditions

$$\left(\frac{\partial}{\partial x} - \mathrm{i}A_x\right)\psi\Big|_{x=0,L_x} = 0, \quad j_{nx}|_{x=0,L_x} = 0 \tag{8}$$

which ensure zero values for both the superconducting and normal components of the current across the boundary, are assumed in the x-direction. In the y-direction, we take the normal metal–superconductor boundary conditions

$$\psi|_{y=0,L_y} = 0, \quad j_{ny}\Big|_{y=0,L_y} = j_e \tag{9}$$

with a uniform density of the externally applied current j_e at the boundaries.

When solving numerically the two-dimensional (2D) version of the TDGL equation (1), the gauge invariance of the discretized equations is preserved by introducing link variables following the method of [34, 35]. The 2D grid, used in our calculations, has 123×243 equally spaced nodes. As described in more detail in [36], the step h_t of the time variable t is automatically adapted in the course of calculation. This adaptation is aimed at minimizing the number of steps in t and—at the same time—to keep the solving procedure accurate. In the present simulations the step h_t is typically $\sim 10^{-5}$ to $\sim 10^{-3}$ depending on a specific distribution of the order parameter. For momentary distributions of the order parameter and the (time-dependent) in-plane vector potential $\langle \mathbf{A}_{2D} \rangle$, an iteration procedure is used to determine from equation (2) the corresponding distribution of the scalar potential φ with a relative accuracy not worse than 10^{-4}. The (time-dependent) vector potential $\langle \mathbf{A}_{2D} \rangle$ and the corresponding link variables are calculated using equation (7).

5. Calculated results

In figure 5(a), the calculated time-averaged electric field $E_{dc} = \langle \varphi_A - \varphi_B \rangle / (y_A - y_B)$ between points A and B (see figure 5(b)) is shown as a function of the increasing density of the applied dc $|j_{dc}|$ current for positive (filled circles) and negative (open triangles) current directions. As seen from the inset of figure 5(a), for positive applied currents (full circles), which cause a Lorentz force acting on vortices in the positive x-direction, the onset of the resistive regime occurs at a significantly smaller value of $|j_{dc}|$ than in the case of negative applied currents (empty triangles), which tend to move vortices in the negative x-direction. This result is natural, because the indentations, which are present at the left ($x = 0$) boundary of the strip, greatly facilitate nucleation of vortices and their entry into the superconductor. Even at current densities quite above the onset of the resistive regime in the case of flat boundaries, vortex entry on the micropatterned boundary takes place exclusively through the vertices of indentations. This is illustrated in figure 4(b), where we plot the distribution of the streaming parameter $S = \left[(t_2 - t_1)^{-1} \int_{t_1}^{t_2} (\partial |\psi|^2 / \partial t)^2 \, dt \right]^{1/2}$, introduced in [37] to visualize the vortex trajectories. In the case of negative applied dc currents, where vortices enter the strip through the flat right ($x = 15 \, \mu\mathrm{m}$) boundary, the entry points for vortices are not well defined. As a result, the corresponding pattern of S (figure 4(c)) appears somewhat smeared out as compared to that shown in figure 4(b).

For comparison, in figure 5(a) we also plot the results calculated for a symmetric strip with flat boundaries at both sides (crosses). As follows from the inset of figure 5(a), in this case the magnitude of the critical current, which corresponds to the onset of the resistive regime,
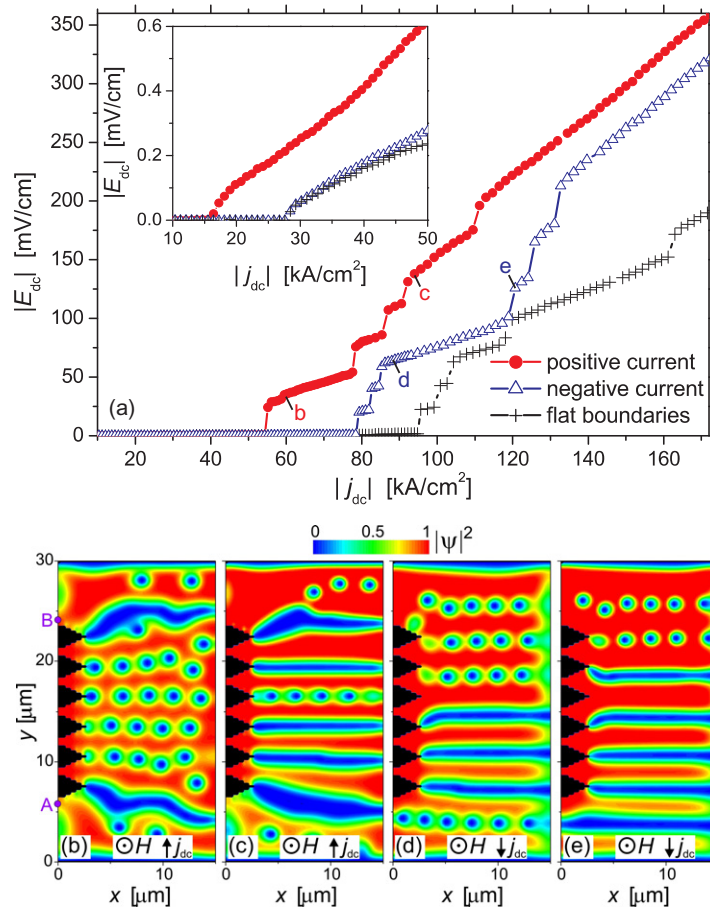
Figure 5. (a) Absolute value of the calculated average electric field E_{dc} between points A and B (see panel (b)) as a function of the increasing density $|j_{dc}|$ of the applied dc current for positive (filled circles) and negative (open triangles) current directions. For comparison, the results for a symmetric bridge with flat boundaries are shown with crosses. Snapshots of the order parameter distributions, which correspond to points labeled as 'b' ($j_{dc} = 59\,\text{kA}\,\text{cm}^{-2}$), 'c' ($j_{dc} = 94\,\text{kA}\,\text{cm}^{-2}$), 'd' ($j_{dc} = -87\,\text{kA}\,\text{cm}^{-2}$) and 'e' ($j_{dc} = -122\,\text{kA}\,\text{cm}^{-2}$), are plotted in panels (b)–(e), respectively. The inset of panel (a) shows the behavior of $E_{dc}(j_{dc})$ at relatively low current densities.

is practically the same as that for negative currents in the strip with indentations shown in figure 4. This clearly demonstrates that the onset of the resistive regime is mainly determined by a possibility for vortices to enter the superconductor and hence by the properties of the 'inlet' boundary of the strip, rather than by the properties of the 'outlet' boundary. However, as seen from a comparison between the results plotted in figure 5(a) with crosses and open triangles, the effect due to patterning of the 'outlet' boundary on the behavior of $E_{dc}(j_{dc})$ above the critical current is not negligible. In particular, such a patterning facilitates the formation of PSLs (see figures 5(b)–(e)), which results in sudden jumps of E_{dc} versus $|j_{dc}|$ (see figure 5(a)). In the case of a patterned 'inlet' boundary, the PSLs appear at even smaller current densities $|j_{dc}|$.

The difference between the curves $E_{dc}(j_{dc})$ for positive and negative current directions (filled circles and open triangles, respectively, in figure 5(a)) implies the appearance of a positive
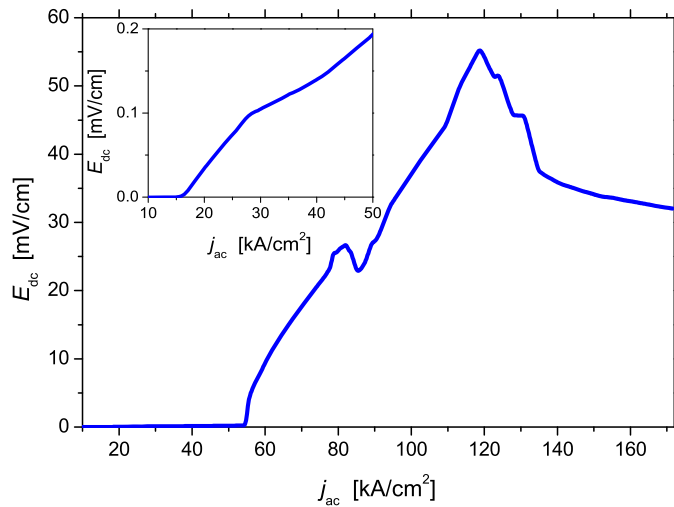
Figure 6. Calculated rectified electric field E_{dc} between points A and B (see figure 5(b)) as a function of the density amplitude j_{ac} of the applied low-frequency ac current. The inset shows the behavior of $E_{dc}(j_{ac})$ at relatively low current densities.

rectified electric field E_{dc} when applying an ac current to the strip. In the limit of low ac frequencies, this rectified electric field (see figure 6) is found using the results for an increasing dc current (figure 5(a)) as well as the curves $E_{dc}(j_{dc})$ calculated for decreasing current densities j_{dc} starting from the values that correspond to different numbers of PSLs (not shown here). A relatively large difference between the current densities, corresponding to the formation of a given number of PSLs at positive and negative current directions (see figure 5(a)), results in a broad peak of $E_{dc}(j_{ac})$ in figure 6. The smaller features on the curve $E_{dc}(j_{ac})$ are related to the change of the number of PSLs formed during the positive/negative half-period of the applied ac current.

6. Discussion

Upon comparing the calculated results with the measured data, we find good qualitative agreement between theory and experiment. In both cases the indented sample manifests a sizable and robust ratchet signal. When comparing figure 6 with figure 2, one can notice that the steep increase of the calculated $E_{dc}(j_{ac})$, caused by the onset of the PSL regime, occurs at an appreciably higher amplitude of the ac current density j_{ac} than that experimentally observed for the indented strip. This discrepancy can be attributed to the difference between the used $\gamma = 10$ and much larger experimental γ-values for Al (indeed, an increase of γ leads to formation of PSLs at lower currents—see e.g. [30]). However, the aforementioned difference in γ-values cannot explain the fact that both the height and the width of the peak in the calculated $E_{dc}(j_{ac})$ are much larger than those observed in the experiment. Indeed, at low ac frequencies an increase of γ tends to increase the magnitude of the rectified field in the PSL regime [25]. It must be mentioned that at high vortex velocities heating effects must not be neglected. Heating could contribute to lowering the currents corresponding to the formation of PSLs for both polarities of the current, therefore lowering the height and width of the measured ratchet signal.

The difference between the calculated and measured shapes of the $E_{dc}(j_{ac})$ peak may also be related to the presence of imperfections on the nominally flat edges of the experimental samples (see figure 1). Indeed, edge defects are known to significantly facilitate the vortex entrance through a rough edge [14, 38]. Due to this effect, the difference between the current densities that correspond to the formation of PSLs for positive and negative currents can be significantly smaller as compared to our model, where the right edge of the superconducting strip is perfectly flat. Correspondingly, the height and width of the measured $E_{dc}(j_{ac})$ peak should be reduced as compared to the calculations for an idealized sample. This explanation is supported by the observation of a relatively well pronounced peak of $E_{dc}(j_{ac})$ on the reference sample with nominally flat boundaries at ac current amplitudes that slightly exceed those for the indented sample (see figure 2). Remarkably, for both the reference and indented samples the measured values of the rectified field E_{dc} still remain comparable to or even larger than the maximum rectified electric fields (few mV cm^{-1}) experimentally obtained for ratchet systems with intentionally introduced arrays of asymmetric antidots [9, 39]. This clearly indicates that the properties of the sample edges may play an important role, also when measuring the rectified voltage on samples with ratchet arrays.

Our TDGL simulations also show that the maximum critical dc current density j_1, corresponding to the onset of vortex propagation across the superconducting bridge shown in figure 4(a), is achieved at a non-zero magnetic field. This confirms earlier predictions [13, 14] for the field dependence of the critical current in a superconducting strip with different vortex-entry conditions at the opposite boundaries. In [13, 14] such different vortex-entry conditions, attributed to different roughnesses of the sample boundaries, were introduced ad hoc by postulating an arbitrarily chosen difference between the two critical current densities for vortex entry at the two opposite sides of the strip. As distinct from the aforementioned model, in the present model a difference between the surface barriers for vortex entry shows up as a direct natural consequence of the engineered sample asymmetry. Due to this well-pronounced asymmetry, in a considerably wide range of magnetic fields around zero the critical density j_1 of a positive dc current appears to be a monotonously decreasing function of H: we find $j_1 = 282$, 231 and 182 kA cm^{-2} for $H = -0.025$, 0 and 0.025 mT, respectively. A relatively large magnitude of the derivative $\partial j_1 / \partial H|_{H=0} \approx -2000$ kA (cm^{-2} mT) implies that an efficient rectification of vortex motion is possible also in the regime where, instead of a dc magnetic field and an ac current, a weak ac magnetic field and a dc current (e.g. with density $j_{dc} \approx 230$ kA cm^{-2}) are applied to the structure under consideration.

7. Conclusions

Summarizing, we report a qualitative and quantitative analysis of rectified electric fields in indented Al bridges. The origin of the ratchet is based on the fact that the onset of vortex motion is mainly governed by the entrance/nucleation of vortices and the current crowding effect produced by the indentations that facilitate this vortex nucleation process. Upon comparing the calculated results with the measured data we find good agreement between theory and experiment. In both cases the indented sample exhibits a sizable and robust ratchet signal. We show that the defects at geometrical borders of a superconducting bridge can play a crucial role in the overall ratchet signal. These effects have been systematically ignored when interpreting the results of ratchet effect measurements performed in samples with arrays of asymmetric

IOP Institute of Physics Φ DEUTSCHE PHYSIKALISCHE GESELLSCHAFT

pinning centers. Our findings point to the need of revising previous investigations, particularly when making quantitative estimations.

Acknowledgments

References

[1] Reimann P 2002 *Phys. Rep.* **361** 57
[2] Hanggi P and Marchesoni F 2009 *Rev. Mod. Phys.* **81** 387
[3] Hanggi P, Marchesoni F and Nori F 2005 *Ann. Phys.* **14** 51–70
[4] Linke H 2002 *Appl. Phys.* A **75** 167
[5] Villegas J E, Savelev S, Nori F, Gonzalez E M, Anguita J V, Garcia R and Vicent J L 2003 *Science* **302** 1188
[6] Van de Vondel J, De Souza Silva C C, Zhu B Y, Morelle M and Moshchalkov V V 2005 *Phys. Rev. Lett.* **94** 057003
[7] de Souza Silva C C, Van de Vondel J, Morelle M and Moshchalkov V V 2006 *Nature* **440** 651
[8] Gillijns W, Silhanek A V, Moshchalkov V V and Reichhardt C 2007 *Phys. Rev. Lett.* **99** 247002
[9] Qiming L, Olson Reichhardt C J and Reichhardt C 2007 *Phys. Rev.* B **75** 054502
[10] Girard J-P, Paumier E and Hairie A 1980 *Phys. Rev.* B **21** 2734
[11] Marchenko V A and Sal'nikov G I 1987 *Surface: Physics, Chemistry, Mechanics* **3** 112 (in Russian)
[12] Lin N S, Heitmann T W, Yu K, Plourde B L T and Misko V R 2011 *Phys. Rev.* B **84** 144511
[13] Plourde B L T, Van Harlingen D J, Vodolazov D Yu, Besseling R, Hesselberth M B S and Kes P H 2001 *Phys. Rev.* B **64** 014503
[14] Vodolazov D Y and Peeters F M 2005 *Phys. Rev.* B **72** 172508
[15] Pryadun V V, Sierra J, Aliev F G, Golubovic D S and Moshchalkov V V 2006 *Appl. Phys. Lett.* **88** 062517
[16] De Souza Silva C C, Silhanek A V, Van de Vondel J, Gillijns W, Metlushko V, Ilic B and Moshchalkov V V 2007 *Phys. Rev. Lett.* **98** 117005
[17] Aliev F G, Levanyuk A P, Villar R, Sierra J F, Pryadun V V, Awad A and Moshchalkov V V 2009 *New J. Phys.* **11** 063033
[18] Bean C P and Livingston J D 1964 *Phys. Rev. Lett.* **12** 14–6
[19] Geim A K, Grigorieva I V, Dubonos S V, Lok J G S, Maan J C, Filippov A E and Peeters F M 1997 *Nature* **390** 259–62
[20] Singha Deo P, Schweigert V A and Peeters F M 1999 *Phys. Rev.* B **59** 6039–42
[21] Drude P 1900 *Ann. Phys.* **1** 566–613
[22] Romijn J, Klapwijk T M, Renne M J and Mooij J E 1982 *Phys. Rev.* B **26** 3648–55
[23] Tinkham M 1996 *Introduction to Superconductivity* 2nd edn (New York: McGraw-Hill)
[24] Leo A, Grimaldi G, Nigro A, Pace S, Verellen N, Silhanek A V, Gillijns W, Moshchalkov V V, Metlushko V and Ilic B 2010 *Physica* C **470** 904–6
[25] Van de Vondel J, Gladilin V N, Silhanek A V, Gillijns W, Tempere J, Devreese J T and Moshchalkov V V 2011 *Phys. Rev. Lett.* **106** 137003
[26] Sabatino P, Carapella G and Gombos M 2012 *J. Appl. Phys.* **112** 083909

IOP Institute of Physics ⚫ DEUTSCHE PHYSIKALISCHE GESELLSCHAFT

[27] Clem J R, Mawatari Y, Berdiyorov G R and Peeters F M 2012 *Phys. Rev.* B **85** 144511

[28] Adami O-A *et al* 2013 *Appl. Phys. Lett.* **102** 052603

[29] Kramer L and Watts-Tobin R J 1978 *Phys. Rev. Lett.* **40** 1041

[30] Vodolazov D Y and Peeters F M 2007 *Phys. Rev.* B **76** 014521

[31] Lawrence W E and Meador A B 1978 *Phys. Rev.* B **18** 1154

[32] Vodolazov D Y, Peeters F M, Morelle M and Moshchalkov V V 2005 *Phys. Rev.* B **71** 184502

[33] Kato R, Enomoto Y and Maekawa S 1991 *Phys. Rev.* B **44** 6916

[34] Kato R, Enomoto Y and Maekawa S 1993 *Phys. Rev.* B **47** 8016

[35] Gropp W D, Kaper H G, Leaf G K, Levine D M, Palumbo M and Vinokur V M 1996 *J. Comput. Phys.* **123** 254

[36] Silhanek A V, Gladilin V N, Van de Vondel J, Raes B, Ataklti G W, Gillijns W, Tempere J, Devreese J T and Moshchalkov V V 2011 *Supercond. Sci. Technol.* **24** 024007

[37] Gladilin V N, Tempere J, Devreese J T, Gillijns W and Moshchalkov V V 2009 *Phys. Rev.* B **80** 054503

[38] Buzdin A and Daumens M 1998 *Physica* C **294** 257

[39] de Souza Silva C C, Van de Vondel J, Zhu B Y, Morelle M and Moshchalkov V V 2006 *Phys. Rev.* B **73** 014507